Original Article

Platelet-rich plasma promotes diabetic ulcer repair through inhibition of ferroptosis

Li Chen[1,2], Daoai Wu[3], Lili Zhou[1,4], Yan Ye[1]

[1]Department of Immunology, School of Basic Medical Sciences, Anhui Medical University, Hefei, China; [2]Department of Blood Transfusion, The First Affiliated Hospital Bengbu Medical College, Bengbu, China; [3]Department of Endocrinology, The First Affiliated Hospital Bengbu Medical College, Bengbu, China; [4]Department of Hematology, The First Affiliated Hospital Bengbu Medical College, Bengbu, China

Contributions: (I) Conception and design: L Chen, Y Ye; (II) Administrative support: L Chen, D Wu; (III) Provision of study materials or patients: L Chen, D Wu, Y Ye; (IV) Collection and assembly of data: L Zhou; (V) Data analysis and interpretation: L Chen, Y Ye; (VI) Manuscript writing: All authors; (VII) Final approval of manuscript: All authors.

Correspondence to: Yan Ye. Department of Immunology, School of Basic Medical Sciences, Anhui Medical University, Hefei, China. Email: yeyan@ahmu.edu.cn.

Background: Ferroptosis, a newly discovered form of cell death, can accumulation activates lipid peroxidation and excessive oxidative stress in a high glucose environment. These phenomena suggest there may be ferroptosis pathways in the pathological processes associated with diabetic ulcer (DU). Platelet-rich plasma (PRP) promotes the healing of DU wounds, which may be achieved by the regulation of ferroptosis pathways. Hence, the present study aimed to investigate this association and uncover the potential underlying mechanisms.

Methods: Cell injury models induced by high glucose were constructed using EA.HY926 (vascular endothelial cells), HSF (fibroblasts), and rat DU models. The MDA, total ROS, total SOD content, the gene and protein expression of *GPX4*, *SLC7A11*, and *ACSL4*, and the expression levels of inflammatory cytokines IL-1β, IL-10, and NLRP3 was subsequently used to evaluate the important role of ferroptosis in the pathological process of DU, and elucidating the molecular mechanism of PRP in ulcer repair.

Results: The results show that compared with the DU control group, the healing rate of the dorsal ulcer wound in the PRP intervention group was accelerated, and the expression levels of inflammatory cytokines IL-1β, IL-10, and *NLRP3* in the granulation tissue of ulcer wounds was lower. Further, the expression levels of *CD31* and *VEGF* were higher, the gene and protein expression levels of *GPX4* and *SLC7A11* were increased, the expression levels of *ACSL4* were less, the SOD content was higher, and the MDA content was lower.

Conclusions: In this study, ferroptosis was preliminarily verified in DUs at the cellular and animal levels, while PRP could inhibit ferroptosis and significantly improve the migration and regeneration ability of fibroblasts and vascular endothelial cells induced by high glucose.

Keywords: Platelet-rich plasma (PRP); ferroptosis diabetic; ulcer healing

Submitted Aug 22, 2022. Accepted for publication Oct 14, 2022.
doi: 10.21037/atm-22-4654
View this article at: https://dx.doi.org/10.21037/atm-22-4654

Introduction

According to the International Diabetes Federation, about 500 million people worldwide suffer from diabetes, and this number is expected to increase by 5% and 51% by 2030 and 2045, respectively. The condition is estimated to be undiagnosed in 50%, approximating 232 million individuals (1). Data from China show 11.2% (according to World Health Organization criteria) or 12.8% (American Diabetes Association criteria, including glycosylated haemoglobin) of Chinese adults aged 18 years and older had diabetes (2) in 2017. Diabetic ulcer (DU) is a serious chronic complication of the disease, and its harm is mainly

manifested as diabetic foot ulcer healing disorders, diabetic foot, gangrene, and even the need for amputation in severe cases (3,4). Common triggers of DFU formation include a high glucose environment, infection, microvascular circulation disorders, a variety of neuropathies, and slow skin tissue regeneration (5). However, the pathogenesis of DFU and the specific molecular pathway of action have not been clarified. Moreover, the long treatment time and high cost not only seriously reduce the quality of life of patients, but create a huge economic on patients, their families and society at large. Therefore, how to effectively prevent and treat DFU is an urgent research issue.

It is well-known that studying cell death patterns plays an important role in elucidating the molecular mechanisms of disease development and provides a scientific theoretical basis for finding safe and effective clinical treatments (6,7). Cell death patterns include programmed death and unprogrammed death, and among the many types of cell necrosis, ferroptosis is a newly discovered form. The main pathological feature of ferroptosis is lipid peroxidation damage involved in a Fenton reaction in the presence of intracellular iron overload. *GPX4* and *SLC7A11* are two characteristic factors associated with the upstream signaling pathway of ferroptosis. *GPX4* is a "scavenger" of lipid peroxides that removes excess intracellular lipid peroxides, while *SLC7A11* is an important component of the glutathione transporter upstream of *GPX4* and promotes intracellular synthesis of glutathione (GSH), a precursor of *GPX4* (8). *ACSL4* is a member of the long-chain fatty acyl coenzyme A synthase family that catalyzes fatty acid activation to synthesize fatty acyl coenzyme A *in vivo* and is a key enzyme in the first step of fatty acid catabolism. Knockdown of enzymes other than *ACSL4* in the *ACSL* family in murine embryonic fibroblasts has not been found to cause ferroptosis (9), and unlike other members of the *ACSL* family, *ACSL4* can activate long-chain polyunsaturated fatty acids to participate in membrane phospholipid synthesis. In addition, inhibition of *GPX4* by lipid peroxides requires (9,10) the involvement of *ACSL4*. These findings suggest *ACSL4* may be a crucial determinant of ferroptosis. Thus, detection of the degree of lipid peroxidation damage, *GPX4*, *SLC7A11*, and *ACSL4*, is important for characterizing the presence or absence of ferroptosis patterns in cells. Moreover, cellular lipid peroxidation injury is not only one of the important markers of ferroptosis, but also plays an important role in the pathological link of DUs (11-14). In a high glucose environment, reactive oxygen species (ROS) production is excessive and GSH synthesis process is blocked, causing *GPX4* content and activity to decrease and resulting in the continuous accumulation of lipid peroxides. This results in cell membrane lipid peroxidation damage, which is an important molecular mechanism of DU repair disorders receiving much attention in recent years. Therefore, ferroptosis may inhibit DU healing.

Platelet-rich plasma (PRP) is the concentration of platelets and plasma extracted from autologous blood by centrifugation, and platelets in PRP can release a variety of growth factors and cytokines after activation (15). Different factors have synergistic effects and are involved in the regulation of cell migration, division, differentiation, tissue angiogenesis, extracellular matrix synthesis, and the vascular repair of damaged tissues during tissue regeneration and repair (16), and the use of PRP has met with good results in the clinical treatment of DUs (17,18). The results of previous clinical study showed PRP could promote granulation tissue proliferation and significantly shorten ulcer healing time in DUs. In addition, HE staining of tissue sections showed a significant increase in fibroblasts and neovascularization, and PRP may be involved in inhibiting cellular ferroptosis pathways. However, the mechanism by which PRP promotes ulcer healing is unknown, and whether it can affect the expression of gene proteins involved in the ferroptosis signaling pathways in DUs has rarely been reported and is the subject of this study. We present the following article in accordance with the ARRIVE reporting checklist (available at https://atm.amegroups.com/article/view/10.21037/atm-22-4654/rc).

Methods

Preparation of PRP

For PRP preparation, about 17.5 mL of blood was collected from the antecubital vein of healthy adult volunteers using a 20-mL syringe preloaded with 2.5 mL sodium citrate anticoagulant and slowly mixed to prevent coagulation. Some samples were obtained to detect the whole blood platelet concentration with an automatic cell counting system within 1 h, and the rest were used for the next experiment. The study was conducted in accordance with the Declaration of Helsinki (as revised in 2013). The study was approved by ethics committee of The First Affiliated Hospital Bengbu Medical College (No. 2021148). Informed consent was taken from all the participants. Blood was slowly injected into two centrifuge tubes, with an average

of about 10ml per centrifuge tube, then centrifuged at 200 g for 10 min at room temperature. The yellowish part in the upper layer and the part 1–2 mm below the middle layer were then carefully pipetted into another centrifuge tube and again centrifuged at 2,500 g for 15 min at room temperature. About two-thirds of the clear liquid in the upper layer was then discarded, with more than 2 mL of the clear liquid retained for final adjustment of the platelet concentration. The remaining 1–2 mL of liquid at the bottom of the centrifuge tube as PRP, was resuspended, and the platelet concentration adjusted using an automatic cell counting system until its concentration reaches 4–5 times that of the whole blood concentration. The PRP was then thoroughly mixed with activator (calcium gluconate, bovine thrombin) at a volume ratio of 9:1), then incubated at 37 ℃ for 1 h to activate it. Activated PRPs were then centrifuged with a table-top centrifuge at 2,000 g for 10 min to remove cell debris and subsequently filtered through a 0.22-pm filter before applied directly or stored in a –80 ℃ freezer until use. In this study, 10 SD rats with successful modeling were anesthetized with 5% chloral hydrate (10 mL/1 kg) intraperitoneally. Pericardium blood samples were collected, and the method steps were the same as above. Animal experiments were performed under a project license (No. 2022289) granted by committee of Bengbu Medical College, in compliance with Bengbu Medical College guidelines for the care and use of animals.

Cell culture

The human skin fibroblasts (HSF) and EA of vascular endothelial cells (EA.HY926) was purchased from Punosai Biotechnology Co., Ltd. Cells were cultured at 37 ℃ in DMEM (Gibco, Carlsbad, CA) containing 10% fetal bovine serum (Gibco, Carlsbad, CA), 100 U/mL penicillin, and streptomycin (Beyotime, Shanghai, China). After recovery and passage of HSF and EA.HY926 cells, 96-well plates (cell density of 2×10^4 cells/mL) were added and cultured in a cell incubator overnight. After removal, high glucose medium containing different concentrations of PRP and Erastin was added to each experimental well of the culture plate to prepare Erastin solutions at final concentrations of 2.5, 5 and 10 μM, and 5%, 10% and 20% PRP solutions, respectively. Of these, HSF cells corresponded to 25 mmol/L of high-glucose medium, and EA.HY926 cells corresponded to 30 mmol/L of high-glucose medium, while control wells were filled with high glucose medium only. The plates were incubated in a cell incubator for 24, 48, and 72 hours (37 ℃, 5% CO_2) then removed, washed three times with PBS solution, and replaced with normal medium without drugs. CCK-8 solution 10 μL/well was then added to each well of a 96-well plate, and the plate was incubated in the dark for 1 hour before removal to detect cell survival. Then (I) a normal control (NC) group, (II) high glucose (HG) group, (III) PRP + high glucose (PRP + HG) group, (IV) Erastin two-hour early intervention + high glucose (Erastin + HG) group, (V) PRP + Erastin two-hour early intervention + high glucose (PRP + Erastin + HG) group, (VI) mannitol hypertonic control (mannitol control) group. In addition, according to the results of CCK-8 assay and combined with the previous exploration of the optimal cell culture time, 10% PRP and 5 μM Erastin were selected as HSF and EA.HY926. The duration of intervention to obtain the required concentration of cells was 48 hours.

Cell viability, scratch assay and mobility assessment

Cell viability was measured using a Cell Counting Kit-8 (CCK-8, MCE, USA) according to the manufacturer's instructions and the percentage cell viability was calculated at each timepoint. The proliferation and migration ability of fibroblasts were observed by cell scratch assay. (I) Cell spreading: 6×10^5 HSF cells were added to each well, and the fusion rate reached 100% after overnight culture. (II) Cell streaking: on the day following cell inoculation and following intervention with HSF from each component of fibrocytes, adherent cells were scratched perpendicular to the horizontal line on the back of the plate using a 200-μL pipette tip. (III) Washing cells: the scratched cells were washed three times with sterile PBS buffer to fully remove the remaining non-adherent cells so the gaps left after scratching were clearly visible. The serum-free medium cell intervention solution of each group was then replaced, and the cells were cultured in an incubator (37 ℃, 5% CO_2). (IV) Cell observation: at the beginning, and after 48 h of culture, the culture plate was removed, observed, and photographed under a light microscope. (V) Analysis of results: using ImageJ software to open the cell photos, six horizontal lines were randomly selected.

Quantitative reverse-transcription PCR

Total RNA was extracted from cells or tissue samples using an HP Toal RNA Kit (Omega Bio-Tek, Norcross, GA) according to the manufacturer's instructions. cDNA synthesized by reverse transcription was reverse transcribed

Table 1 Primers used for qPCR

Gene	Forward	Reverse
GPX4	GAGGCAAGACCGAAGTAAACTAC	CCGAACTGGTTACACGGGAA
SLC7A11	TCTCCAAAGGAGGTTACCTGC	AGACTCCCCTCAGTAAAGTGAC
ACSL4	CATCCCTGGAGCAGATACTCT	TCACTTAGGATTTCCCTGGTCC

qPCR, quantitative polymerase chain reaction.

according to the reaction temperature and time program. After mixing all reactants and rapid centrifugation once, the mixture was placed in a preheated PCR instrument, the reaction procedure started, and the data read. Primer sequences are presented in *Table 1*.

Western blot analysis

Cells and tissues were lysed using radioimmunoprecipitation assay (RIPA) lysis buffer (Solarbio, Beijing, China). Protein samples were collected according to the instructions to ensure the loading amount of protein samples in each well was consistent. After SDS-PAGE gel preparation, sample processing, loading and electrophoresis, transfer to membrane, blocking, and incubation with primary antibodies against GPX4 (59735S, CST, USA), *SLC7A11* (12691S, CST, USA), *ACSL4* (ab155282, abcam, USA), *CD31* (3528S, CST, USA), *VEGF* (ab52917, abtime, USA) or *GAPDH* (60004-1-Ig, Proteintech, China). The membranes were then incubated with secondary antibody, and the photos were taken in the gel imaging system.

ROS evaluation

DCFH-DA (Solarbio, Beijing, China) was diluted using serum-free culture medium at a dilution ratio of 1:1,000. The cell culture medium was aspirated and discarded, and after HSF and EA.HY926 cells were intervened, 1 mL/well DCFH-DA dilution was added to the six-well plate. After stimulation in the cell culture incubator at 37 ℃ for 40 min, the original culture medium was aspirated and discarded, an appropriate amount of serum-free cell culture medium was added, and the cells were manually washed five times for 10 minutes each time to fully remove excess DCFH-DA. After counterstaining with DAPI solution (Solarbio, Beijing, China), intracellular ROS levels were measured by detecting the intensity of DCF fluorescence using a confocal laser scanning microscope with an excitation wavelength of 502 nm and an emission wavelength of 530 nm.

Enzyme-linked immunosorbent assay analysis

The protein levels of IL1β, IL6, *NLRP3* in tissue homogenates were measured with IL1β Rat ELISA Kit (PI305, beyotime, China), IL6 Rat ELISA Kit (D6050, rndsystems, USA), *NLRP3* Rat ELISA Kit (abcam, USA), respectively. The concentrations of MDA, SOD was conducted using MDA Kit (S0131S, Beiotime, China), SOD Kit (S0101S, Beiotime, China) according to the manufacturer's instructions.

Animals

All experimental animals were eight-week-old male Sprague-Dawley rats (SCXK, Hangzhou, China) weighing 220–250 g. They were housed in polycarbonate cages at room temperature (21–23 ℃) with a 12-h light/dark cycle and 60–70% humidity. Animal study was performed under the ethical committee of Bengbu Medical College. After 1 week, the dose of STZ solution required for each experimental rat was calculated at 65 mg/kg, and intraperitoneal injection was performed. Blood samples were collected from the tail vein of all model rats 3 days after drug injection, and blood glucose was measured by glucometer and test strip. A random blood glucose level greater than or equal to 16.7 mmo/L was used as a marker of successful modeling.

Establishment of wound model

Diabetic SD rats with a back ulcer model were anesthetized by intraperitoneal injection of 5% chloral hydrate at 10 mL/kg. After the ventral surface of the rats was fixed downward, the back was shaved and disinfected. A round full-thickness skin defect wound model with a diameter of 1.5 cm was cut on both sides of the back vertebrae. According to the different treatment methods, 30 rats were divided into six groups (n=5): (I) a PRP-treated group which received local injection of PRP into the ulcer every 3 days; (II) a saline-

treated group, which received the same amount of 0.01% DMSO sterile saline injected into the ulcer base every 3 days; (III) a ferroptosis inhibitor-treated group, which received 2 mg/kg of the ferroptosis inhibitor ferrostatin-1 containing 0.01% DMSO sterile saline into the ulcer base every 3 days; (IV) a diabetic control group (diabetes control), in which no local intervention was applied to the ulcer; (V) a healthy control group, which received no local intervention to the ulcer; (VI) a normal saline treatment group, in which the same amount of 0.01% DMSO sterile saline was injected into the ulcer base every 3 days.

Evaluation of ulcer wound healing rate in diabetic rats

Wound size changes, healing time, and wound conditions were observed and recorded every day following the establishment of the DU model. The formula for calculating the ulcer wound healing rate C% of animals was as follows:

$$C\%=\left[(C0-Ct)/C0\right]\times 100\% \quad [1]$$

where C0 is the ulcer area on the first day after surgery and Ct is the ulcer area on the last day of the experiment.

Hematoxylin and Eosin staining and immunohistochemistry (IHC)

On day 10, after skin wounding, all rats were euthanized by pentobarbital sodium overdose, and the wound tissues were excised and fixed in 4% paraformaldehyde. Hematoxylin and Eosin (H&E) staining was performed for analysis of tissue inflammation including neutrophils and phagocytes, and the morphological and quantitative changes of fibroblasts, vascular endothelial cells, and epithelial cells under a light microscope, and the pathological characteristics were observed at tissue and cellular levels. IHC staining of proteins was performed by incubation of sections with 5% normal goat serum for 1 h followed by incubation overnight with primary antibodies against IL-1β (PI305, beyotime, China), IL6 (D6050, rndsystems, USA), *NLRP3* (abcam, USA), respectively. The sections were washed three times with PBS, incubated with secondary antibodies (Vector Laboratories, Burlingame, CA) for 2 h at room temperature, incubated with horseradish peroxidase (HRP)-diaminobenzidine (DAB) reagents (Proteintech, Wuhan, China), and then counterstained with hematoxylin. Sections were analyzed by light microscopy (Carl Zeiss Microscopy International, Germany), and images were analyzed using the Image-Pro Plus 6.0 software.

Statistical analysis

GraphPad Prism 8.0 was used to statistically analyze the experimental data. All quantitative results are expressed as mean ± SD, and unpaired two-tailed Student *t*-test was used for statistical analysis. Differences between groups were analyzed by one-way ANOVA followed by Tukey's post-test.

Results

High glucose-induced lipid peroxidation injury model of cell membrane

Cell viability under different drug concentrations was evaluated to investigate the effect of the ferroptosis inhibitor PRP and inducer Erastin on the fibroblast HSF and vascular endothelial cell EA.HY926 in a high glucose environment. Different culture conditions were applied to the two different cells with the concentration and time of related drugs set, and the cell survival rate was detected by CCK-8 assay. The results showed the cell survival rate increased with the increase of PRP concentration in the same culture time range and increased with the increase of PRP concentration in the intervention of the same drug concentration. In addition, at a certain concentration of Erastin, the survival rate of cells decreased with the prolongation of the treatment time of the inducer Erastin, and at a certain concentration of Erastin, the survival rate of cells decreased with the increase of the drug concentration of Erastin (*Figure 1A-1D*).

Gene and protein expression of ferroptosis markers in the cell model of high glucose injury induced by PRP were detected according to the results of CCK-8 assay. Combined with the previous exploration of the optimal cell culture time, 10% PRP and 5 μM Erastin were used as the cell intervention concentrations of HSF, and 10% PRP and 5 μM Erastin were used as EA. The cell intervention time was 48 h. Following the previous intervention, we used real-time PCR to detect the gene expression of *GPX4*, *SLC7A11*, and *ACSL4* in cells, and as shown in the figure, *GPX4* and *SLC7A11* were down-regulated and ACSL4 was up-regulated in cells in the high glucose group compared with the normal control group. In addition, the gene expression of *GPX4* and *SLC7A11* was significantly up-regulated and ACSL4 was down-regulated in cells in the PRP + Erastin intervention group (PRP + Erastin + high glucose) compared with the high glucose group (high glucose) ($P<0.001$); the gene expression of *GPX4* and *SLC7A11* was significantly up-regulated in cells in the

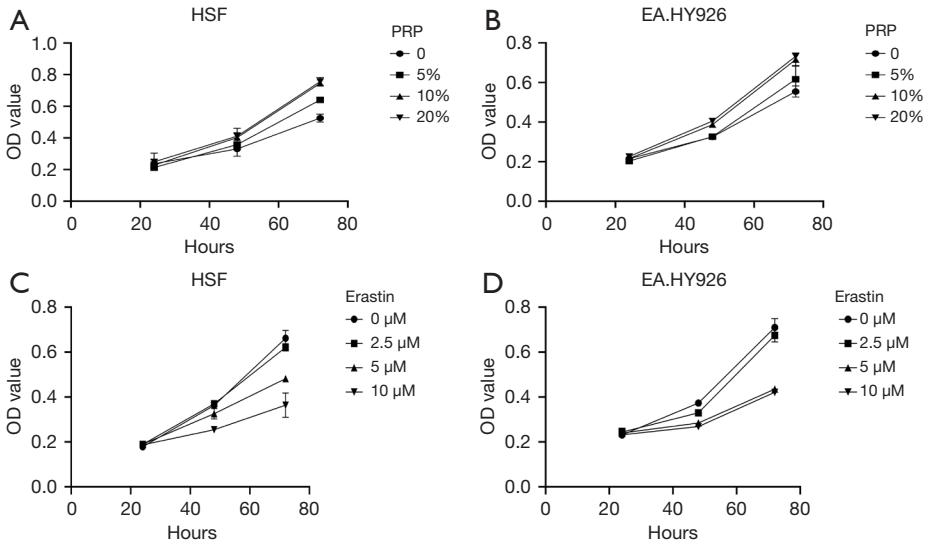

Figure 1 PRP and inhibition of ferroptosis in HSF and EA.HY926 cells exposed to HG conditions. (A,B) The CCK-8 detection results of PRP on HSF and EA.HY926 cells. It can be seen that within the same culture time range, with the increase of PRP, the cell survival rate showed an increasing trend. Under the intervention of the same drug concentration, the cell survival rate increased with the prolongation of the treatment time of PRP. (C,D) The effect of Erastin on the survival rate of HSF and EA.HY926 cells. It can be seen that the survival rate of cell decreases with the extension of the duration of Erastin when the drug concentration is fixed. With the increase of Erastin concentration, the survival rate of fibroblast HSF decreased. OD, optical density; PRP, platelet-rich plasma; HSF, human skin fibroblasts; HG, high glucose.

PRP + Erastin intervention group (PRP + Erastin + high glucose) compared with the inducer intervention group (Erastin glucose) (P<0.01); and the gene expression of ACSL4 was significantly down-regulated in cells in the high glucose group compared with the high glucose group and the inducer intervention group (Erastin glucose) (P<0.001 and P<0.01, respectively. The results of these experiments showed *GPX4* and *SLC7A11* gene expression was down-regulated and *ACSL4* gene expression was up-regulated in a high glucose environment, and the intervention of Erastin, a ferroptosis inducer, could aggravate this trend. Further the intervention of PRP significantly improved the characteristic related indicators of ferroptosis and significantly up-regulated the gene expression of *GPX4* and *SLC7A11*, while down-regulating the *ACSL4* expression. In addition, there was no significant difference in the expression of ferroptosis-related genes between the hypertonic control group (mannitol control) and the high glucose group (high glucose), indicating the experiment was not affected by glucose hyperosmolality (*Figure 2A-2D*). Based on these intervention conditions and experimental groups, we further used Western blot technique to detect the protein expression of the intracellular ferroptosis markers *GPX4*, *SLC7A11*, and *ACSL4* in each experimental group, and the results were consistent with the *qRT-PCR* results (*Figure 2A-2D*).

Effects of PRP on lipid peroxidation injury in the high glucose injury cell model are as follows. Based on the above intervention conditions and experimental groups, we then used confocal laser scanning technology and ELISA to detect the degree of lipid peroxidation injury in each experimental group, and the results showed that compared with the high glucose group (PRP + high glucose), the PRP treatment group (PRP + high glucose) cells and Erastin + high glucose group had the highest fluorescence quantification results and the highest total ROS fluorescence intensity, while EA in the PRP + high glucose and PRP + Erastin + high glucose groups was similar to the Erastin + high glucose group. While quantification of total ROS fluorescence intensity was significantly decreased in EA.HY926 cells (P<0.001) the, total intracellular ROS was significantly increased in the PRP + Erastin + high glucose group compared with the normal control group (P<0.00l) (*Figure 3A*). The MDA content of EA.HY926 seen in the Erastin + high glucose group had the highest intracellular MDA content of 2.523 nmol/mL, which was significantly higher than EA.HY926 in the PRP + high glucose group MDA content

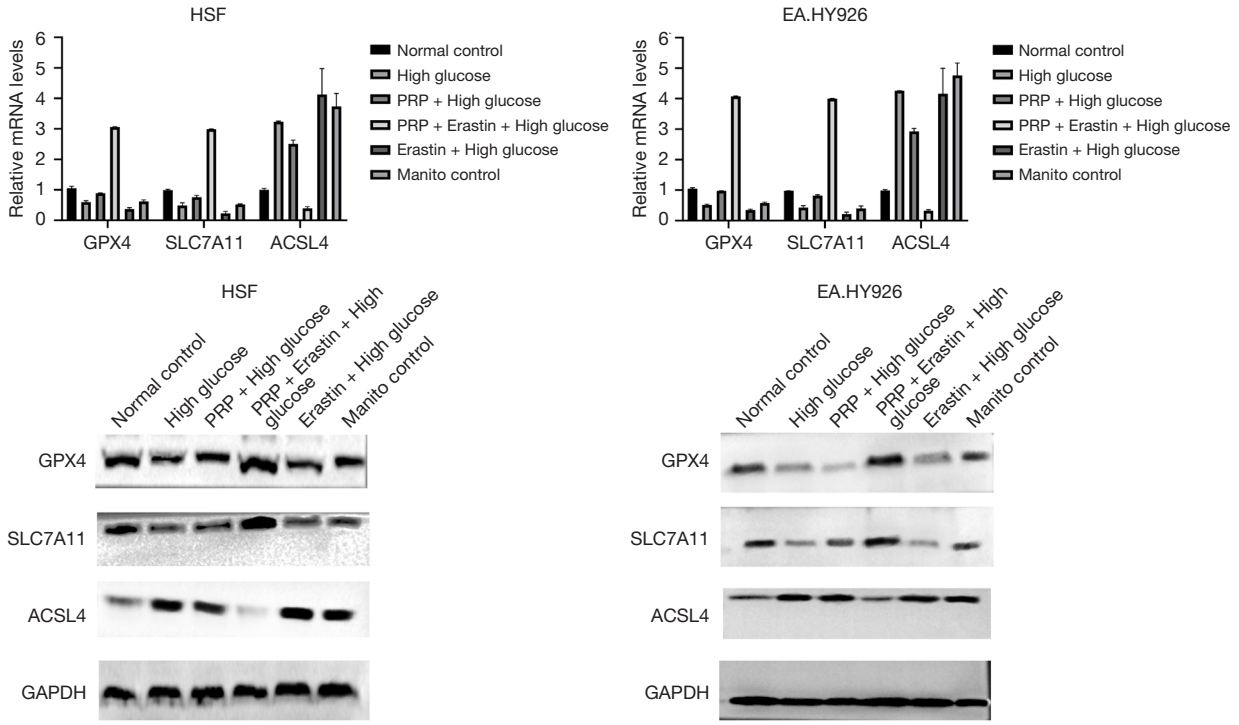

Figure 2 Real-time PCR and protein expression detection results of ferroptosis markers *GPX4*, *SLC7A11* and *ACSL4*. In high glucose environment, the expression of *GPX4* and *SLC7A11* genes was down-regulated, and the expression of *ACSL4* gene was up-regulated. The intervention of ferroptosis inducer Erastin could aggravate the change trend, and the intervention of PRP significantly improved the related indicators of iron death, and significantly up-regulated the expression of *GPX4* and *SLC7A11* genes. The expression of ACSL4 was also down-regulated. HSF, human skin fibroblasts; PRP, platelet-rich plasma; PCR, polymerase chain reaction.

(P<0.05) EA within each intervention group. In the PRP + high glucose group, the content of SOD in EA.HY926 cells was 22.13 nU/mL, which was significantly higher than in the Erastin + high glucose group SOD content in EA.HY926 cells (P<0.05). These findings suggest high concentrations of glucose aggravate fibroblast EA and lipid peroxidation damage within hy926, and intervention with Erastin, an ferroptosis inducer, further exacerbates lipid peroxidation damage, while PRP can effectively reduce it in vascular endothelial cells due to high glucose concentrations (*Figure 3B,3C*).

The effect of PRP intervention on fibroblast proliferation and migration ability is shown as the mobility of fibroblast HSF observed under a light microscope after different intervention treatments. Quantification and statistical results of cell migration rates using Image J software showed HSF cells had the highest migration rate of 67% among the six experimental groups in the PRP + high glucose group. The lowest migration rate was in the Erastin + high glucose group, which was only 20%, followed by the high glucose group with 27%. Among them, cell proliferation mobility was significantly increased in the PRP + high glucose group compared with the Erastin + high glucose group (P<0.001) and was significantly lower in the high glucose and PRP + Erastin + high glucose groups (P<0.01). These results showed the proliferation mobility of HSF in fibroblasts was decreased in a high glucose environment, that Erastin would further reduce the proliferation and migration of HSF in fibroblasts in a high glucose environment, and PRP would significantly improve the proliferation mobility of HSF in fibroblasts in this environment (*Figure 4A,4B*).

The effect of PRP intervention on the regenerative capacity of vascular endothelial cells is shown in the figure, and CD31 and VEGF protein expression was significantly increased in the PRP + high glucose group compared with the high glucose and Erastin + high glucose groups (P<0.05, P<0.01, and P<0.001, respectively). Compared with the Erastin + high glucose group, the intracellular VEGF content of EA.HY926 cells in the PRP + Erastin + high glucose group was significantly increased (P<0.001), and compared with

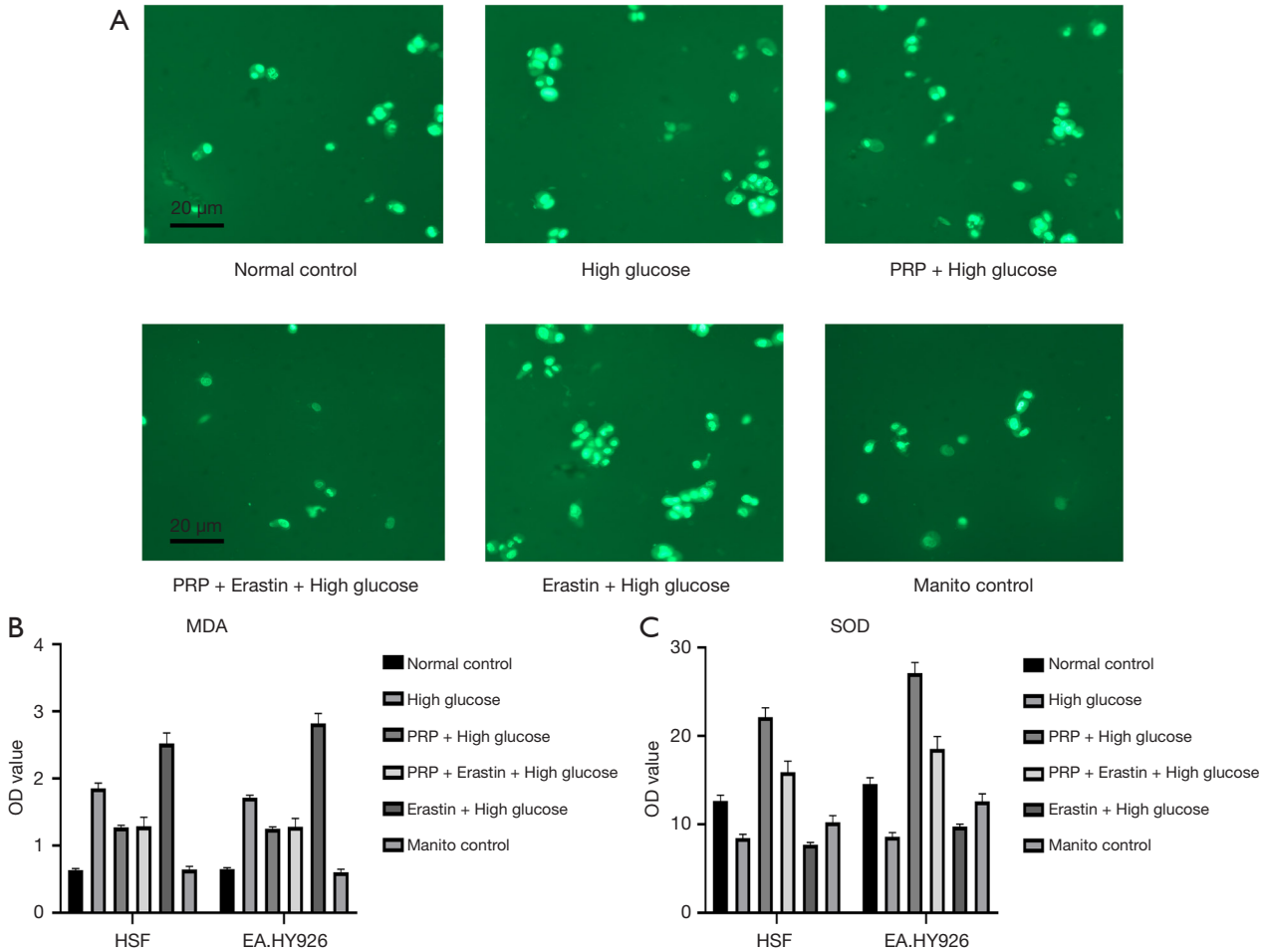

Figure 3 The degree of lipid peroxidation damage was detected in each intervention group. Compared with the high glucose group, in the PRP treatment group (PRP + high glucose), the Erastin + high glucose group had the highest fluorescence quantification result and the highest total ROS fluorescence intensity. Compared with Erastin + high glucose group, the quantified values of intracellular ROS fluorescence intensity in EA.HY926 cells in PRP + high glucose group and PRP+ Erastin + high glucose group were significantly decreased (P<0.001). Compared with Normal control group, the total intracellular ROS in PRP + Erastin + high glucose group was significantly increased (P<0.001) (A). The MDA content of EA.HY926 seen in the Erastin + high glucose group had the highest intracellular MDA content of 2.523 nmol/mL, which was significantly higher than EA.HY926 in the PRP + high glucose group MDA content (P<0.05) EA within each intervention group. The SOD content of EA.HY926 cells in each intervention group was the highest in PRP + high glucose group—22.13 nU/mL, which was significantly higher than the SOD content in Erastin + high glucose group (P<0.05) (B,C). PRP, platelet-rich plasma; OD, optical density; MDA, malonic dialdehyde; HSF, human skin fibroblasts; SOD, superoxide dismutase; ROS, reactive oxygen species.

the normal control group and the mannitol control group, the expression of CD31 and VEGF protein in EA.HY926 cells was decreased in the high glucose group. These results suggest the regeneration ability of vascular endothelial cell EA.HY926 is decreased in a high glucose environment, that Erastin further aggravates the low regeneration ability of vascular endothelial cells in this environment, and that PRP can significantly improve the regeneration ability of vascular endothelial cells (*Figure 5A-5C*).

PRP promotes ulcer healing in diabetic rats and its mechanism

PRP increases the re-epithelialization rate of ulcer wounds in diabetic rats

To investigate whether PRP could promote ulcer wound

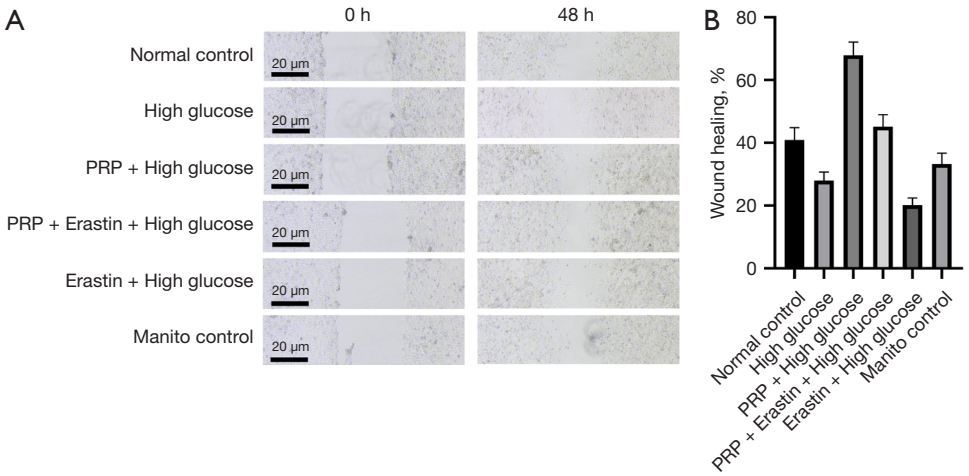

Figure 4 Examination of HSF migration ability of fibroblasts. In PRP + high glucose group, HSF cells had the highest migration rate, and Erastin + high glucose group had the lowest migration rate, followed by high glucose group. Compared with the Erastin + high glucose group, the cell proliferation and migration rate in the PRP + high glucose group was significantly increased (P<0.001). Compared with the PRP + Erastin + high glucose group, the cell proliferation and migration rate in the PRP+ Erastin + high glucose group was significantly increased (P<0.001). The cell proliferation and migration rates were significantly lower (P<0.01) (A,B). PRP, platelet-rich plasma; HSF, human skin fibroblasts.

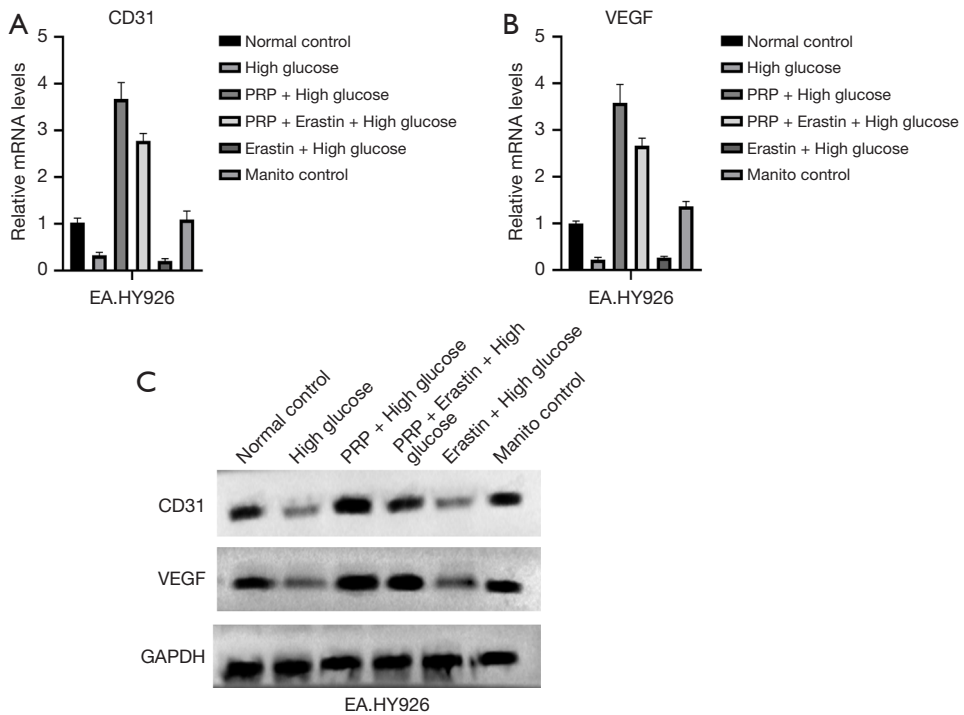

Figure 5 Detection of regeneration ability of vascular endothelial cells EA.HY926. Western blot analysis of CD31 and VEGF of vascular endothelial cells in each group. (A) Compared with the high glucose group and Erastin + high glucose group, the protein expressions of CD31 and VEGF in PRP + high glucose group were significantly increased (P<0.05, P<0.01 and P<0.001, respectively). (B) Compared with Erastin + high glucose group, VEGF content in EA.HY926 cells in PRP+ Erastin + high glucose group was significantly increased (P<0.001). (C) Compared with Normal control group and Manito control group, the protein expressions of CD31 and VEGF in EA.HY926 cells in high glucose group were decreased. PRP, platelet-rich plasma; VEGF, vascular endothelial growth factor; GAPDH, glyceraldehyde-3-phosphate de hydrogenase.

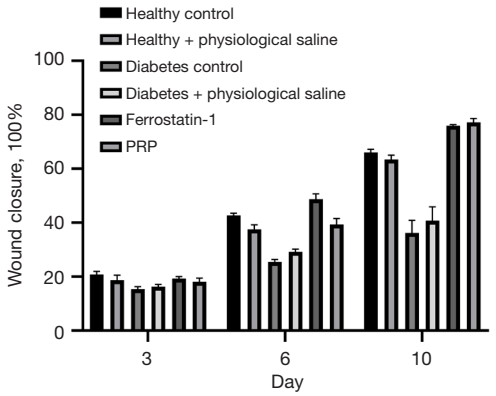

Figure 6 PRP for ulcer repair in diabetic rats: results of re-epithelialization rate assessment in each group. After PRP was injected into the ulcer wound at the bottom of the ulcer, the healing rate of the back ulcer of diabetic rats was significantly increased, and the re-epithelialization rate was significantly higher than that of diabetic rats in the same period on the 3rd, 6th, and 10th day of medication (P<0.001). PRP, platelet-rich plasma.

healing in diabetic rats, a 10-day *in vivo* animal experiment was conducted. According to the statistical results of the re-epithelialization rate shown in *Figure 6*, after PRP was injected into the ulcer wound at its bottom, the healing rate was significantly increased, and on the 3rd, 6th, and 10th day of treatment, the re-epithelialization rate was significantly higher than in diabetic rats at the same time (P<0.001). Further, this even reached the state of being flat with the re-epithelialization rate of back ulcers in healthy rats. These results show PRP injected into the ulcer wound through the ulcer bottom can effectively promote the healing of back ulcer wound in rats.

PRP alleviated ulcer inflammation in diabetic rats

The recruitment of inflammatory cells in granulation tissue of the dorsal ulcer skin was observed by HampE staining on the 3rd, 6th, and 10th day of intervention, and the contents of inflammatory cytokines IL-1β, IL-6, and NLRP3 were quantitatively detected by ELISA.

After the 10th day of PRP intervention, HampE staining observation results revealed red areas as normal cells, blue as nuclei, and purple as inflammatory cells, and showed that in the untreated diabetic rat ulcer group (diabetes control) and saline treatment group, a large area of purple inflammatory cell infiltration was present. In contrast, a large area of inflammatory cell infiltration was not observed in the local application of PRP to the ulcer wound (*Figure 7A-7C*), and this result was consistent with the HampE staining results of the ulcer wound tissue in the healthy rat group. This indicated PRP could effectively inhibit the activity of inflammatory cells in the ulcer wounds of diabetic rats. However, the ELISA protein contents of inflammatory cytokines IL-1β, IL-10, and NLRP3 in the PRP injection group (PRP injection) were about 0.83, 0.84, and 0.91 pg/mL, respectively, which were numerically closest to those in the normal rat control group (1.01, 1.04, and 1.03 pg/mL, respectively). In addition, the contents of IL-1β and IL-10 in the PRP-treated group were significantly lower than in the saline-treated group (P<0.01, P<0.05, respectively) and diabetic rat group (diabetes control) (P<0.01, P<0.05, respectively) (*Figure 7D,7E*). These findings suggest the local application of PRP to diabetic rat dorsal ulcers significantly inhibits inflammatory cell activity, attenuates the production of inflammatory factors, and promotes vascular and skin regeneration and repair in tissues.

PRP decreased the content of MDA and increased the content of SOD in the skin granulation tissue of ulcer in diabetic rats

PRP decreased the content of MDA and increased the content of SOD, which could indirectly reflect the degree of lipid peroxidation injury in the granulation tissue of rat back ulcers. In general, the results of SOD and MDA content in the granulation tissue of the ulcer skin of diabetic rats in each group after PRP intervention on the 10th day. In general, after the local application of PRP, the MDA content in granulation tissue of ulcerated skin of diabetic rats was the lowest, about 0.37 nmol/g, and the SOD content was the highest, about 17.48 nU/mL, which were numerically similar to those of normal healthy rats. Further, the MDA content was significantly lower than that of diabetic rats (diabetes control) and saline-treated groups, and the SOD content was significantly higher than that of diabetic rats (diabetes control) and saline-treated groups, (both P<0.001). These experimental results showed PRP significantly decreased MDA content and significantly increased SOD content in the granulation tissue of ulcerated skin in diabetic rats, effectively reducing lipid peroxidation damage in granulation tissue (*Figure 8A,8B*).

Gene and protein expression of ferroptosis-related factors in granulation tissue of ulcerated skin

To further verify the presence of ferroptosis, a cell death

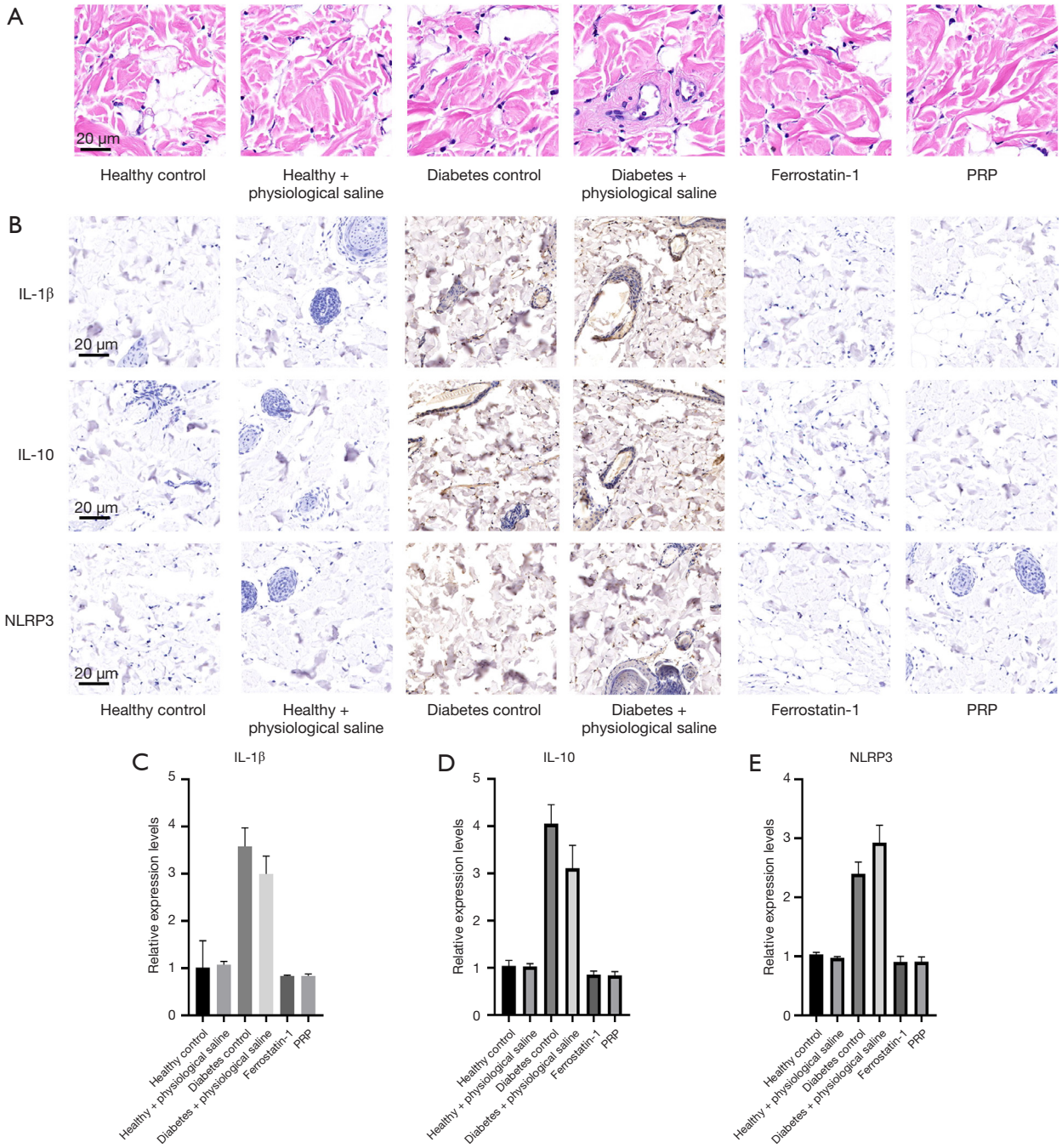

Figure 7 The repair function of PRP on diabetic rats ulcer. (A,B) In the results of H&E staining, normal cells are shown in red, nuclei are shown in blue, and inflammatory cells are shown in purple. It can be seen that large areas of purple inflammatory cells are infiltrated in both untreated diabetic rats in the ulcer control group and saline treatment group. On the contrary, no large area of inflammatory cell infiltration was observed in the PRP group (A,B). The ELISA results of protein content detection of inflammatory factors IL-1β, IL-10 and NLRP3 in skin granulation tissue of ulcer. The levels of IL-1β, IL-10 and NLRP3 in the skin granulation tissue of ulcers in PRP injection group were about 0.83, 0.84 and 0.91 pg/mL, respectively, which were the most similar to those of normal rats control (1.01, 1.04, 1.03 pg/mL, respectively), and the levels of IL-1β and IL-10 in PRP treatment group were significantly lower than those in normal saline treatment group ($P<0.01$, $P<0.05$, respectively) and diabetes group ($P<0.01$, $P<0.05$, respectively) (C-E). PRP, platelet-rich plasma; H&E, hematoxylin and eosin; ELISA, enzyme linked immunosorbent assay; IL-1β, interleukin-1β; IL-10, interleukin-10; NLRP3, nucleotide-binding oligomerization domain, leucine-rich repeat and pyrin domain-containing protein 3.

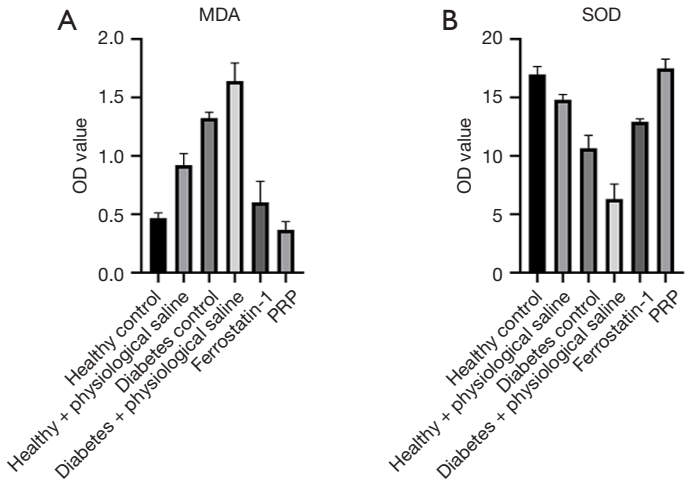

Figure 8 Changes of MDA and SOD contents in skin tissue of ulcerative skin of rats after PRP drying. (A) On the 10th day after PRP intervention, the content of MDA in the skin granulation tissue of ulcer of diabetic rats was the lowest, about 0.37 nmol/g, and the content of SOD was the highest, about 17.48 nU/mL, which were similar to those of normal healthy rats. (B) The content of MDA was significantly lower than that in diabetes control group and saline treatment group, and the content of SOD was significantly higher than that in diabetes control group and saline treatment group (all P<0.001). MDA, malonic dialdehyde; OD, optical density; PRP, platelet-rich plasma; SOD, superoxide dismutase.

pattern, in the granulation tissue of the dorsal ulcer skin of diabetic rats, we detected the gene and protein expression of ferroptosis-related factors *GPX4*, *SLC7A11*, and *ACSL4* of each experimental group by fluorescence quantitative PCR and Western blot. Using *GAPDH* as an internal reference, the PCR detection results showed the gene expression levels of *GPX4* and *SLC7A11* in granulation tissue were up-regulated after PRP intervention and were significantly higher than those in the diabetic rat group (all P<0.001). In contrast, *ACSL4* gene expression was significantly lower in PRP-treated rats than in saline-treated rats and diabetic rats (P<0.001), which was consistent with the ferroptosis inhibitor (Ferrostatin-1) group (*Figure 9A-9C*).

Taking *GAPDH* as an internal reference, *GPX4*, *SLC7A11*, and *ACSL4* results of Western blot were as shown. After PRP intervention, the protein expression of *GPX4* and *SLC7A11* in the granulation tissue of the ulcerated skin of diabetic rats was up-regulated, and was significantly higher than that of the normal saline treatment group and diabetes control group (both P<0.001), and *ACSL4* in the PRP-treated group. The protein expression level in diabetic rats was also lower than in the normal saline treatment group and diabetes control group, which was consistent with the ferrostatin-1 group (*Figure 9D*).

Discussion

It is well-known that epithelial cells have excessive apoptosis and a low ability to regenerate and migrate, and that the ability of endothelium cells to regenerate and proliferate is reduced and collateral circulation is difficult to establish. All of these are important factors that lead to the prolongation of wound healing in DUs (19-21). A high concentration of glucose increases the production of peroxide in the cell and converts into lipids which combine with the peroxide to form a continuous supply and excessive production of lipid peroxidation. If not removed in a timely manner, this can cause cell dysfunction or even death (22-25). Ferroptosis is a recently discovered form of cell death characterized by lipid peroxidation damage involving iron or lipoxygenase, which attacks biological macromolecules and ultimately induces cell death. This implies lipid peroxidation injury is an important pathological mechanism of refractory DU wounds and may be closely related to the pathway of ferroptosis. *GPX4*, *SLC7A11*, and *ACSL4* are the characterizing factors of ferroptosis (9,26). In a high glucose environment, HSF, and endothelium EA.HY926 lipid peroxidation injury, the expression of ferroptosis related factors *GPX4* and *SLC7A11* genes and proteins were up-regulated compared with a normal glucose concentration, while expression of *ACSL4* genes and proteins was down-

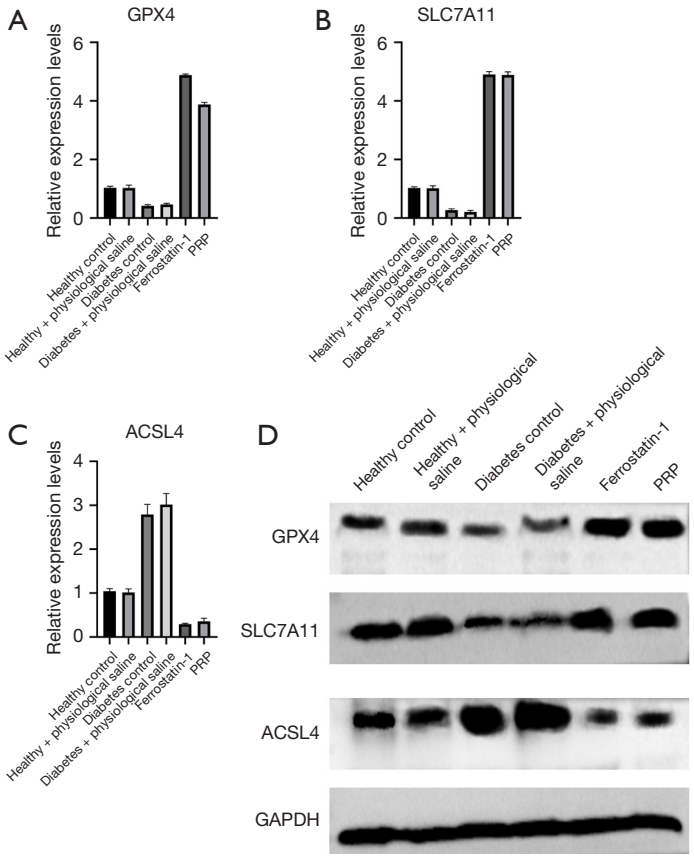

Figure 9 Real-time PCR and protein expression detection results of ferroptosis markers GPX4, SLC7A11 and ACSL4. After PRP intervention, the gene expressions of GPX4 and SLC7A11 in the skin granulation tissue of ulcer of diabetic rats were up-regulated, which were significantly higher than those of diabetes control rats (all P<0.001). In contrast, the expression of ACSL4 in PRP group was significantly lower than that in saline group and diabetes control group (both P<0.001) (A-C). The results were consistent with the protein expression results (D). PCR, polymerase chain reaction; PRP, platelet-rich plasma.

regulated. These results support our previous hypothesis that in a high-glucose environment, fibroblast HSF and endothelium EA.HY926 may undergo iron-related lipid peroxidation injuries. As an inducer of ferroptosis, Erastin targets *GPX4* and is a small molecule inhibitor of *GPX4*. In this study, PRP was added to Erastin-induced hyperglycemic cells, either fibroblast HSF or endothelium EA.HY926. Compared with Erastin, the expression levels of *GPX4* and *SLC7A11* were up-regulated, while the content of lipid peroxidation and the expression levels of *ACSL4* were down-regulated, suggesting PRP can inhibit the cell ferroptosis induced by Erastin. In addition, while the gene and protein expressions of *GPX4* and *SLC7A11* were up-regulated in PRP-treated high glucose cells compared with those in non-treated high glucose cells, the content of lipid peroxidation and the expression level of *ACSL4* were down-regulated. This confirmed PRP could alleviate the damage of lipid peroxidation and inhibit HSF and endothelium EA.HY926 induced by high glucose ferroptosis. These results suggest the proliferation and migration of fibroblast HSF and endothelium EA.HY926, and the regeneration ability of hy926 decreases in a high glucose environment. Combined with the above analysis, it can be seen that the cell death induced by high glucose will further cause cell dysfunction. Furthermore, the above findings suggest high glucose-induced cellular ferroptosis can be inhibited by PRP, and in the group of high glucose cells with PRP intervention compared with those without, the migration and proliferation of fibroblast HSF were increased. This indicates PRP can inhibit high glucose-induced cell ferroptosis and promote the proliferation of fibroblast HSF and endothelium EA.HY926.

PRP is a platelet concentrate containing large amounts of proteins and growth factors prepared after whole blood centrifugation. Activated PRP has a three-dimensional network of microstructures as a biologically active scaffold (fibrin gel) which is conducive to cell migration and new matrix formation (27). Based on these advantages, PRP has been widely used to promote skin regeneration, colon anastomosis, and bone formation (28,29), and the study has shown that PRP treatment induces the proliferation and growth activity of cells are enhanced after external radiation (30). PRP has been found to have a similar effect in human skin fibroblasts, and given its role in promoting the migration and proliferation of skin fibroblasts, it is capable of being used to treat patients with chronic injuries (31). In addition, a series of important research results revealed an increase of local tissue glutathione content could promote granulation tissue regeneration and accelerate wound healing in diabetic animal models of ulcer under hyperglycemia (32-34). In this study, the ulcer healing rate of diabetic rats was significantly increased after PRP was injected into the bottom of the ulcer, and the ulcer healing rate was significantly increased at the 3rd, 6th, and 10th day after injection. The re-epithelialization rate was significantly higher than that of diabetic rats ($P<0.001$), and even reached the same level as that of healthy rats, indicating injection of PRP at the bottom of an ulcer could effectively promote its healing. In addition, the present study found the iron-related death signature factors *GPX4* and *SLC7A11* in the wound surface of DU rats were downregulated in gene and protein expression compared with those after PRP use, while *ACSL4* showed an up-regulation trend. Further, after RPP intervention, the content of lipid peroxidation MDA and inflammatory factors IL-1β, IL-10, and NLRP3 decreased, but that of SOD was adversed. Therefore, we hypothesized that ROS are produced in tissues and cells at high glucose levels, and that as more glucose enters the cells, lipid peroxidation production increases. Further, that under the action of iron ions in the cells, lipid peroxidation can accumulate and attack DNA and other biomolecules in the granulation tissue of ulcerated skin and trigger cell ferroptosis. PRP can reduce lipid peroxidation damage by activating certain signaling pathways to block the ferroptosis pathway and promote endothelium and epithelial cell regeneration, differentiation and migration, effectively improving the healing ability of ulcer wounds in diabetic rats.

In conclusion, in a high-glucose environment, fibroblast HSF and endothelium EA.HY926 can undergo ferroptosis. The main characteristics are aggravation of lipid peroxidation injury, decrease of *GPX4* and *SLC7A11*, and increase of *ACSL4*. PRP can inhibit the development of ferroptosis, alleviate lipid peroxidation damage in cells, and further promote the development of HSF and endothelium EA.HY926 in proliferation, migration, and regeneration. After local application of PRP, the degree of lipid peroxidation injury in granulation tissue cells, the activity of inflammatory cells and the production of inflammatory factors were significantly reduced in diabetic rats with back ulcers. PRP can increase the gene and protein expression of *GPX4* and *SLC7A11*, decrease the gene and protein expression of *ACSL4*, and further promote the regeneration and repair of skin tissue and microvessels of ulcer wounds, accelerating the healing of back ulcers in diabetic rats. From this, it can be determined that ferroptosis plays a role in the pathological mechanism of skin granulation tissue in diabetic rats, and PRP can inhibit this. By regulating the expression of characteristic factors related to ferroptosis, it can promote the regeneration and repair of blood vessels in ulcer wounds and accelerate healing.

Acknowledgments

Funding: This work was supported by the Scientific Research Project of Bengbu Medical College (No. 2020byzd112).

Footnote

Reporting Checklist: The authors have completed the ARRIVE reporting checklist. Available at https://atm.amegroups.com/article/view/10.21037/atm-22-4654/rc

Data Sharing Statement: Available at https://atm.amegroups.com/article/view/10.21037/atm-22-4654/dss

Conflicts of Interest: All authors have completed the ICMJE uniform disclosure form (available at https://atm.amegroups.com/article/view/10.21037/atm-22-4654/coif). The authors have no conflicts of interest to declare.

Ethical Statement: The authors are accountable for all aspects of the work in ensuring that questions related to the accuracy or integrity of any part of the work are appropriately investigated and resolved. The study was conducted in accordance with the Declaration of Helsinki (as revised in 2013). The study was approved by ethics committee of The First Affiliated Hospital Bengbu

Medical College (No. 2021148). Informed consent was taken from all the participants. Animal experiments were performed under a project license (No. 2022289) granted by committee of Bengbu Medical College, in compliance with Bengbu Medical College guidelines for the care and use of animals.

References

1. Saeedi P, Petersohn I, Salpea P, et al. Global and regional diabetes prevalence estimates for 2019 and projections for 2030 and 2045: Results from the International Diabetes Federation Diabetes Atlas, 9th edition. Diabetes Res Clin Pract 2019;157:107843.
2. Li Y, Teng D, Shi X, et al. Prevalence of diabetes recorded in mainland China using 2018 diagnostic criteria from the American Diabetes Association: national cross sectional study. BMJ 2020;369:m997.
3. Mastrogiacomo M, Nardini M, Collina MC, et al. Innovative Cell and Platelet Rich Plasma Therapies for Diabetic Foot Ulcer Treatment: The Allogeneic Approach. Front Bioeng Biotechnol 2022;10:869408.
4. Oneto P, Etulain J. PRP in wound healing applications. Platelets 2021;32:189-99.
5. Al-Mohaithef M, Abdelmohsen SA, Algameel M, et al. Screening for identification of patients at high risk for diabetes-related foot ulcers: a cross-sectional study. J Int Med Res 2022;50:3000605221087815.
6. Zhang J, Li F, Augi T, et al. Platelet HMGB1 in Platelet-Rich Plasma (PRP) promotes tendon wound healing. PLoS One 2021;16:e0251166.
7. Qi M, Zhou Q, Zeng W, et al. Growth factors in the pathogenesis of diabetic foot ulcers. Front Biosci (Landmark Ed) 2018;23:310-7.
8. Nguyen TT, Ding D, Wolter WR, et al. Validation of Matrix Metalloproteinase-9 (MMP-9) as a Novel Target for Treatment of Diabetic Foot Ulcers in Humans and Discovery of a Potent and Selective Small-Molecule MMP-9 Inhibitor That Accelerates Healing. J Med Chem 2018;61:8825-37.
9. Sha W, Hu F, Xi Y, et al. Mechanism of Ferroptosis and Its Role in Type 2 Diabetes Mellitus. J Diabetes Res 2021;2021:9999612.
10. Shimbara-Matsubayashi S, Kuwata H, Tanaka N, et al. Analysis on the Substrate Specificity of Recombinant Human Acyl-CoA Synthetase ACSL4 Variants. Biol Pharm Bull 2019;42:850-5.
11. Feng J, Wang J, Wang Y, et al. Oxidative Stress and Lipid Peroxidation: Prospective Associations Between Ferroptosis and Delayed Wound Healing in Diabetic Ulcers. Front Cell Dev Biol 2022;10:898657.
12. Li S, Li Y, Wu Z, et al. Diabetic ferroptosis plays an important role in triggering on inflammation in diabetic wound. Am J Physiol Endocrinol Metab 2021;321:E509-20.
13. Dham D, Roy B, Gowda A, et al. 4-Hydroxy-2-nonenal, a lipid peroxidation product, as a biomarker in diabetes and its complications: challenges and opportunities. Free Radic Res 2021;55:547-61.
14. Jelic MD, Mandic AD, Maricic SM, et al. Oxidative stress and its role in cancer. J Cancer Res Ther 2021;17:22-8.
15. Elghblawi E. Platelet-rich plasma, the ultimate secret for youthful skin elixir and hair growth triggering. J Cosmet Dermatol 2018;17:423-30.
16. Wu PI, Diaz R, Borg-Stein J. Platelet-Rich Plasma. Phys Med Rehabil Clin N Am 2016;27:825-53.
17. Leme KC, Neri GM, Biscaro GG, et al. Full Diabetic Foot Ulcer Healing and Pain Relief Based on Platelet-Rich-Plasma gel Formulation Treatment and the Involved Pathways. Int J Low Extrem Wounds 2022. [Epub ahead of print]. doi: 10.1177/15347346221109758.
18. Henning PR, Grear BJ. Platelet-rich plasma in the foot and ankle. Curr Rev Musculoskelet Med 2018;11:616-23.
19. den Dekker A, Davis FM, Kunkel SL, et al. Targeting epigenetic mechanisms in diabetic wound healing. Transl Res 2019;204:39-50.
20. Mponponsuo K, Sibbald RG, Somayaji R. A Comprehensive Review of the Pathogenesis, Diagnosis, and Management of Diabetic Foot Infections. Adv Skin Wound Care 2021;34:574-81.
21. Díaz-Rodríguez E, Agra RM, Fernández ÁL, et al. Effects of dapagliflozin on human epicardial adipose tissue: modulation of insulin resistance, inflammatory chemokine production, and differentiation ability. Cardiovasc Res 2018;114:336-46.
22. Basu Mallik S, Jayashree BS, Shenoy RR. Epigenetic modulation of macrophage polarization- perspectives in diabetic wounds. J Diabetes Complications 2018;32:524-30.

23. Li M, Wang T, Tian H, et al. Macrophage-derived exosomes accelerate wound healing through their anti-inflammation effects in a diabetic rat model. Artif Cells Nanomed Biotechnol 2019;47:3793-803.
24. Maiorino M, Conrad M, Ursini F. GPx4, Lipid Peroxidation, and Cell Death: Discoveries, Rediscoveries, and Open Issues. Antioxid Redox Signal 2018;29:61-74.
25. Liu J, Yang J. Uncarboxylated osteocalcin inhibits high glucose-induced ROS production and stimulates osteoblastic differentiation by preventing the activation of PI3K/Akt in MC3T3-E1 cells. Int J Mol Med 2016;37:173-81.
26. Wu J, Minikes AM, Gao M, et al. Intercellular interaction dictates cancer cell ferroptosis via NF2-YAP signalling. Nature 2019;572:402-6.
27. Pulcini S, Merolle L, Marraccini C, et al. Apheresis Platelet Rich-Plasma for Regenerative Medicine: An In Vitro Study on Osteogenic Potential. Int J Mol Sci 2021;22:8764.
28. Gan F, Wang R, Lyu P, et al. Plasma-Derived Exosomes Boost the Healing of Irradiated Wound by Regulating Cell Proliferation and Ferroptosis. J Biomed Nanotechnol 2021;17:100-14.
29. Hu ZB, Chen HC, Wei B, et al. Platelet rich plasma enhanced neuro-regeneration of human dental pulp stem cells in vitro and in rat spinal cord. Ann Transl Med 2022;10:584.
30. Reinders Y, Felthaus O, Brockhoff G, et al. Impact of Platelet-Rich Plasma on Viability and Proliferation in Wound Healing Processes after External Radiation. Int J Mol Sci 2017;18:1819.
31. Hashemi SS, Mahmoodi M, Rafati AR, et al. The Role of Human Adult Peripheral and Umbilical Cord Blood Platelet-Rich Plasma on Proliferation and Migration of Human Skin Fibroblasts. World J Plast Surg 2017;6:198-205.
32. Sakai O, Uchida T, Imai H, et al. Glutathione peroxidase 4 plays an important role in oxidative homeostasis and wound repair in corneal epithelial cells. FEBS Open Bio 2016;6:1238-47.
33. Friedmann Angeli JP, Conrad M. Selenium and GPX4, a vital symbiosis. Free Radic Biol Med 2018;127:153-9.
34. Sakai O, Yasuzawa T, Sumikawa Y, et al. Role of GPx4 in human vascular endothelial cells, and the compensatory activity of brown rice on GPx4 ablation condition. Pathophysiology 2017;24:9-15.

(English Language Editor: B. Draper)

Cite this article as: Chen L, Wu D, Zhou L, Ye Y. Platelet-rich plasma promotes diabetic ulcer repair through inhibition of ferroptosis. Ann Transl Med 2022;10(20):1121. doi: 10.21037/atm-22-4654

